Effect of Cr, Mo and Ti on the microstructure and Vickers hardness of multicomponent systems

C.D. Gómez-Esparza, J. Camarillo-Cisneros, I. Estrada-Guel, J.G. Cabañas-Moreno, J.M. Herrera-Ramírez**, R. Martínez-Sánchez**

Abstract

This study reports the synthesis of multi-component systems by mechanical alloying, their subsequent consolidation by conventional sintering followed by mechanical and microstructural characterization. Three multi-component systems were selected and the effect of Cr, Mo and Ti is reported. Mechanical alloying leads to formation of nanocrystalline powder alloys of about 5–25 nm after 10 h of milling. XRD patterns indicate the presence of several solid solution phases with BCC and FCC structures in both the as-milled and the sintered products. After the sintering process, new equilibrium phases are crystallized from milled powder. Crystallized phases present simple structures (BCC and FCC) but with some differences in composition, besides tetragonal and/or rhombohedral structures in alloys with Cr and Mo. High hardness values are found in consolidated samples. Alloying elements, grain size, proportion and nano size of dispersed phases have an important effect on mechanical properties.

1. Introduction

The metallic alloys are primarily based on a major element, with additions of other elements in smaller quantities to promote in-creased structural and mechanical performance. It is well known that the addition of several major elements in traditional metallurgy causes the formation of intermetallic compounds and complex

microstructures, which analysis is more difficult. Furthermore the mechanical properties of these alloys decrease with the presence of the typical brittleness of intermetallic compounds.

The multi-component systems (MCS), which are also called high entropy (HE) alloys, were developed by Yeh and co-workers [1]. With at least five elements in equiatomic or near equiatomic compositions, it is expected for these alloys to have excellent proper-ties such as high hardness, good ductility and high temperature stability. This is because of the HE alloys have a tendency to form solid solutions instead of intermetallic compounds due to high entropy of mixing [2–5]. The Gibbs free energy is defined as$\Delta G = \Delta H - T\Delta S$, where H is the enthalpy, S is the entropy, T is the absolute temperature. According to Thermodynamics, the phases with a lower ΔG will be formed permanently. If the enthalpy is constant, the phases with higher entropy will have the lowest free energy. The entropy of a solid solution phase is much higher than that of an intermetallic phase; the atomic structure of a solid solution is randomly formed whereas in an intermetallic phase the structure has an order. As a result, the Gibbs free energy of a solid solution phase is lower than in an intermetallic phase, and thus a solid solution will be more probable to form.

One of the main parameters that affects both microstructural and mechanical properties of MCS is the chemical composition. The AlCoCrCuFeNi alloy is one of the most MCS investigated in the last decade; a proper chemical composition design performed on this alloy can result in better properties. Additions of alloying elements have direct effect on physical and chemical properties. However, each element has a main effect in a determined property; alloys even have similar characteristics of

these elements (structure, atomic radii, melting point, etc.). It has been reported that Cu (FCC) additions, which present high ductility, enhance the plasticity in MCS [6]; while, the mechanical properties such as hard-ness, are mainly improved by additions of Al (FCC), which presents a low melting point, low hardness and high ductility, enhancing the hardness of MCS in an important way. This could be explained because Al promotes the formation of a BCC structure in MCS [1]. However, it is expected that the characteristics of Cr (BCC) like high melting point, high hardness and low ductility have a direct and positive effect in the hardness of MCS [7].

Most reported studies involve liquid processing routes, such as arc melting and casting, melt-spinning [8–10]. However, solid state processing routes are not studied deeply. In this concern, the mechanical alloying (MA), which is a solid state process, has been widely recognized as an alternative processing route to synthesize alloys. Materials produced by MA present nanocrystalline micro-structure and unusual properties [11].

This research is focused on synthesizing 3 different MCS, NiCoAlFeCr, NiCoAlFeMo and NiCoAlFeTi by MA. The effect of the chemical composition, processing parameters on microstructural and structural evolution and the hardness of milled and consolidated alloys are reported and discussed.

2. Materials and methods

A series of three multi-component systems, NiCoAlFeCr, NiCoAlFeMo and NiCoAlFeTi, were synthesized by mechanical alloying (MA). Equiatomic mixtures of commercial pure elemental powders (purity better than 99 wt.%) were mechanically alloyed in a high-energy shaker mill (SPEX-8000M) during 10 h, under an argon atmosphere to avoid oxidation. Hardened steel vial and grinding media were used. A charge ratio of ˜5:1 was used. Methanol was added as a process control agent to avoid excessive agglomeration of particles. Bulk alloys samples were pre-pared by uniaxial pressing at room temperature and 1.5 GPa. The green compacted samples were vacuum sealed in pre-cleaned quartz ampoules and sintered at 1473 K during 3 h, and cooled down into the furnace up to room temperature.

The microstructural features were investigated by field emission scanning electron microscopy (SEM) using a JEOL JSM-7401F microscope. Transmission electron microscopy (TEM) thin-foil specimens were prepared by focused ion beam using a JEM-9320FIB equipped with an Omniprobe 200 nanomanipulator. The composition of the phases was analyzed by an aberration-corrected JEOL-JEM2200FS transmission electron microscope. The X-ray diffraction (XRD) tests were carried out in a Panalytical X'Pert PRO diffractometer with Cu Ka radiation (λ = 0.15406 nm), using 35 kV and 25 mA. The step and acquisition time were 0.01° and 260 s, respectively.

A microhardness test was performed in a Vickers hardness tester CLEMEX MMTX-7. The microhardness values were determined on the polished cross-section of samples with a normal load of 200 g and a dwell time of 10 s. The final hardness

value was averaged by 10 tests.

3. Results and discussion

3.1. Microstructural and structural characterization of the as mechanically alloyed powders

The effect of milling parameters on microstructure is an important issue, which could help in the understanding of each element behavior during processing. The representative microstructures of the mechanically alloyed powders are shown in Fig. 1. Lamellar microstructure is observed in all cases, which was formed by the continuous effect of cold welding and fracture. It is a typical characteristic of the mechanically alloyed materials [11]. MCS NiCoAlFeCr microstructure is shown in Fig. 1a, apparently non dissolved Cr phase, which is dispersed into coarse lamellar microstructure, here shown. The MCS NiCoAlFeMo microstructure is observed in Fig. 1b. An addition of Mo produces a finer microstructure. Small regions containing Mo dispersed into a fine lamellar microstructure are observed in this figure. The effect of Ti additions on lamellar microstructure in milled products is observed in Fig. 1c. It is evident the low dissolution of different elements and the presence of different phases containing differences in composition also dispersed in a coarse lamellar microstructure. The alloy containing Mo had the higher lamellar refinement. This may be caused by the initial particle size of Mo (<20 μm), which is relatively smaller than those of Cr (<50 μm) and Ti (<80 μm). Furthermore, Mo has a greater hardness than Cr and Ti, which promotes fracturing predomination during MA and lamellar refinement increases.

Possible variations in nominal compositions are evaluated by microanalyses.

These variations may be caused by the loss of materials by mechanical drag or material being fastened into milling media. The results of elemental chemical composition of the mechanically alloyed powders are summarized in Table 1. Even when the total X-ray production in EDS analyses depends on both the atomic number of the detecting element in the sample and the operating voltage, the elements with lower atomic number will pro-duce a lower flux of X-rays [12]. The semi-quantitative analyses, which could present relative errors in the order of ±3%, are useful to know the possible deviations from nominal composition. On Table 1 is shown that all elements present different concentration levels than nominal, being the lower variation in Ti and the maximum in Mo. In base composition (NiCoAlFe), Al shows the higher lost after milling and Ni the lower. However, with the exception of Al and Mo, deviations about the nominal concentration were lower than 2 at. %.

According to SEM/EDS mappings (not reported here) performed in the polished cross-section of samples, Cr is concentrated in regions with thickness of about 1 μm (Fig. 1a), while Mo is detected in bright lamellae with thicknesses less than 0.5 μm (Fig. 1b), whereas Fe tends to be homogeneously distributed in the mechani-cally alloyed powders, except in the NiCoAlFeTi alloy, where Fe-rich lamellae are observed (Fig. 1c). This alloy has the lowest homogeneity in chemical distribution. Besides, bright Co-rich areas and thicker dark areas (⩾6 μm) with a high content of Ti–Al–Ni are observed.

The structural and microstructural evolutions after milling process are followed by XRD. The XRD patterns of the powders in the as-milled (10 h of milling, Fig. 2a–c) condition are shown in Fig. 2. The complete disappearance of elemental peaks is

evident within 10 h of milling. The XRD patterns show broad and short peaks denoting a microstructure refining; additionally some higher intensity peaks showed a shift to lower or higher values of 2θ, because of the formation of solid solutions by the dissolution of some elements. These formed solid solutions phases (Fig. 2) exhibit BCC and FCC structures according to the typical patterns of these structures. This structural behavior can be attributed to the solid solubility extension during MA, in comparison with similar alloys produced by melting and casting, mainly in alloys containing Mo [13].

The structure identification, crystallite size, lattice parameters and micro-strains found in MCS after 10 h of milling are reported in Table 2. The lattice parameters of the FCC phases of NiCoAlFeCr and NiCoAlFeMo alloys are 0.353 and 0.354 nm, respectively, which are very close to that of pure Ni (0.352 nm). For the alloy containing Ti, the FCC phase has a lattice parameter (0.441 nm) greater than the other two alloys, which does not correspond to a Ni-like phase, but rather to an Al-like phase (aAl fcc = 0.404 nm). Titanium has an apparent major affinity with Al and promotes the formation of an Al-like FCC phase. It is supposed that the different atomic size of Ti (0.146 nm) respect to Cr and Mo (0.127 and 0.139 nm, respectively) alters the cell-size with a major distortion

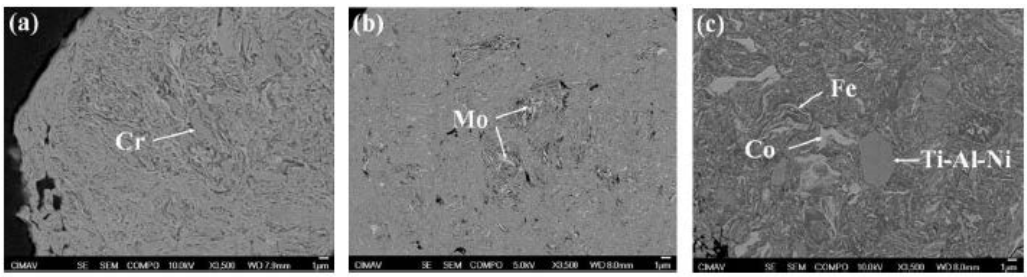

Fig. 1. Backscattered electrons SEM images of the powder samples cross-section: (a) NiCoAlFeCr, (b) NiCoAlFeMo and (c) NiCoAlFeTi.

Table 1
Chemical composition of the mechanically alloyed powders determined by SEM/EDS technique.

Powder alloy	at.%						
	Ni	Co	Al	Fe	Cr	Mo	Ti
NiCoAlFeCr	19.7	20.7	17.5	20.6	21.5		
NiCoAlFeMo	21.0	22.6	17.6	21.7		17.1	
NiCoAlFeTi	21.5	21.5	16.4	20.5			20.1

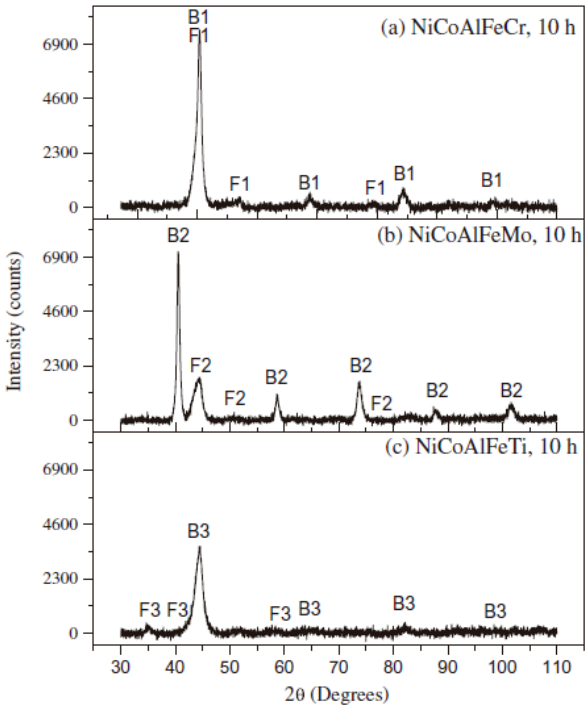

Fig. 2. XRD patterns from the as-milled powders after 10 h.

Table 2
Structural features of powders after 10 h of milling, obtained from XRD patterns.

Alloy	Phase	Lattice parameter (nm)	Crystallite size (nm)	Lattice strain (%)
NiCoAlFeCr	*B1* (BCC)	0.287	10.9	0.944
	F1 (FCC)	0.354	24.5	0.473
NiCoAlFeMo	*B2* (BCC)	0.314	17.6	0.675
	F2 (FCC)	0.353	4.9	1.990
NiCoAlFeTi	*B3* (BCC)	0.288	5.6	1.738
	F3 (FCC)	0.441	10.3	1.264

Causing both, an increment in the lattice parameter (shift to lower angles) and lattice strain.

In the alloys containing Cr and Ti, the lattice parameter of the BCC phases (0.287 and 0.288 nm, respectively) corresponds to a Fe-like BCC phase (aFe bcc = 0.286 nm). For the NiCoAlFeMo alloy, the lattice parameter of the BCC phase is slightly larger (0.314 nm), presenting the characteristics of a Mo-like BCC phase (aMo bcc = 0.315 nm).

3.2. Microstructural characterization of sintered products

The equilibrium microstructure of sintered samples was investigated by scanning and transmission electron microscopy (SEMTEM), shown in (Fig. 3a–c). The qualitative elemental distribution of phases was analyzed by elemental SEM/EDS maps, while chemical composition was determined by TEM/EDS.

Elemental distribution obtained by SEM/EDS mapping analyses revealed that after the sintering process, the alloying elements are not homogeneously distributed. The elements tend to be concentrated in preferential regions and crystallizing new phases, which have different composition (Table 3).

The consolidated products present three main phases identified by contrast and EDS semi-quantitative microanalyses. A discontinuous dark phase (A) is shown on the alloy containing Cr (Fig. 3a), which has a high content of Ni and Al, and low Cr content (<4 at.%). The other two phases observed are a rounded gray phase (C) immersed into a bright and continuous phase (B); both of them have low Al content and mainly differ in the Ni and Cr content. Co and Fe are homogeneously distributed.

It was observed a dark phase (A) in the NiCoAlFeMo alloy (Fig. 3b), which has a high Ni and Al content, while the content of Co and Fe was always close to the nominal concentration. The presence of Mo is lower than 1 at. % in this phase. Phase B is prefer-ably formed by Co and Fe, with medium Ni content and low percentage of Al and Mo. The brightest phase (C) has the highest concentration of Mo (˜45 at.%), the Co and Fe contents are close to the nominal concentration; while, Ni and Al present concentrations lower than 10 at.%.

The representative microstructure of the NiCoAlFeTi alloy is shown in Fig. 3c. It consists of a continuous phase (A), with well de-fined grain boundaries and chemical composition close to the equiatomic (Table 3), except for the Ti content, which is in a lower concentration than the rest of the elements. Zone B is a bright phase with high Co and Fe contents. The spherical, dark precipitates (C) are composed mainly of Ti (>90 at. %) and are found in the intergranular section of phase A.

Thin TEM specimens (<100 nm of thickness) are great candidates to be analyzed by EDS technique and obtain the semi-quantitative chemical composition of their phases with a minor error. The phases indicated in the TEM images of Fig. 4 correspond to the zones indicated in the SEM images of Fig. 3. Accordingly, the results, shown in Table 3, also correspond to those phases. TEM observations were used to identify the range of the matrix grain size and the precipitates formed during the sintering process. The presence of micron and mostly sub-micron crystalline grains, were observed in the samples cross-section by TEM images. Significant grain growth occurred during the sintering process. A close observation reveals that

the size of finer precipitates is mostly in nanoscale. In all the alloys, nanometric aluminum oxide particles were observed. In the alloys with Cr and Ti, the precipitates are non-uniformly dispersed in the whole sample, while they are homogenously distributed in the NiCoAlFeMo alloy (Fig. 4g–i). It is important to emphasize that according to chemical compositions (Table 3), solid solution phases were formed in-stead of the intermetallic compounds predicted by the binary alloy phase diagrams [14]. However, in the MCS the formation of some compounds with high enthalpy of formation such as oxides, carbides and nitrides is also expected [15]. In high-temperature alloys, binary systems or more complex commercial alloys basically composed of Ni, Co and Fe with Al, the formation of protective aluminum oxide scales is desired. The formation of aluminum oxide is dependent of temperature (˜1150 °C) and aluminum content. The addition of chromium promotes the formation of Al2O3 scales [16]. In the studied alloys, the aluminum content and the sintering temperature promote the formation of aluminum oxides that act as reinforcing nanoparticles. This is another strengthening mechanism that improves the hardness of studied alloys.

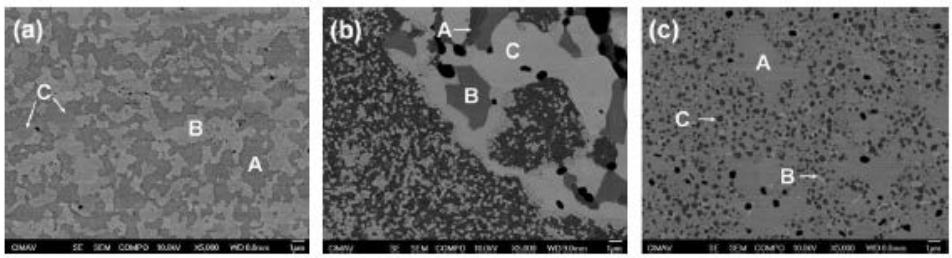

Fig. 3. Backscattered electrons SEM images of the sintered products: (a) NiCoAlFeCr, (b) NiCoAlFeMo and (c) NiCoAlFeTi.

Table 3
Chemical compositions of the sintered alloys according to TEM/EDS analyses.

Sintered alloy	Phase	at.%						
		Ni	Co	Al	Fe	Cr	Mo	Ti
NiCoAlFeCr	*A*	38.46	19.02	26.01	13.12	3.39		
	B	16.01	24.68	3.50	27.63	28.38		
	C	6.30	20.47	3.20	22.59	47.44		
NiCoAlFeMo	*A*	34.94	19.39	27.10	18.18		0.39	
	B	24.34	28.35	7.02	34.55		5.74	
	C	8.58	19.71	6.82	18.46		46.42	
NiCoAlFeTi	*A*	23.34	24.23	16.53	24.03			11.87
	B	7.29	23.02	2.45	65.26			1.99
	C	1.20	1.14	1.84	1.26			94.55

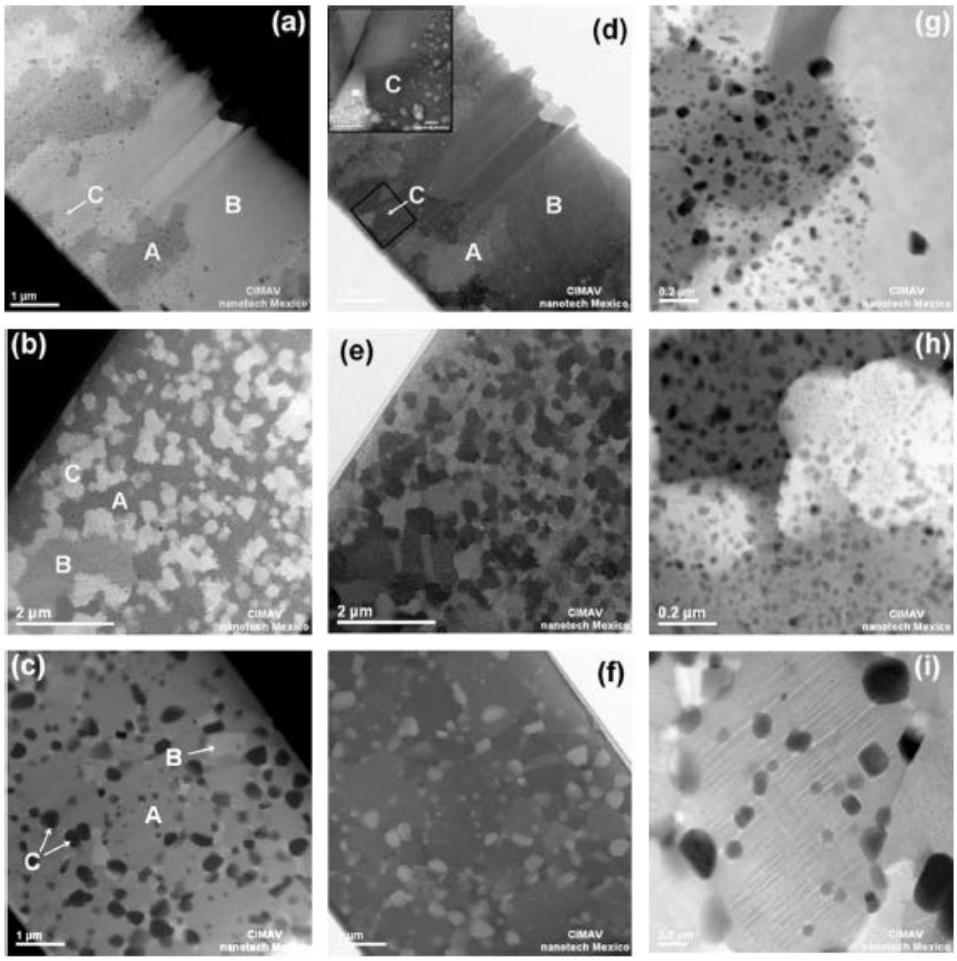

Fig. 4. Z-contrast (left images) and bright-field (center images) scanning TEM images (STEM) showing the microstructure of the sintered samples: (a) NiCoAlFeCr, (b) NiCoAlFeMo and (c) NiCoAlFeTi. Right images correspond to Z-contrast TEM images at high magnifications.

3.3. Structural characterization of sintered products

X-ray diffraction patterns of the sintered products reveal the presence of BCC and FCC crystalline solid solution phases (Fig. 5). According to the lattice parameter measurements (Table 4), the NiCoAlFeCr has a lattice parameter of 0.358 nm and 0.287 nm for the FCC and BCC solid solution phases, respectively. Previous investigations reported the same equiatomic alloy, but produced by vacuum arc melting, which only possessed a BCC structure with a lattice constant of ≈0.287 nm [17,18]. Contrary to Al0.3CoCrFeNi alloy produced by induction melting and casting, and subsequent aging treatment at 900°C, that exhibits B2 ordered solid solution phase precipitated in a FCC matrix [19]. Also, the studied alloy has the presence of a group of other diffraction peaks (Fig. 5a), which is referred by some authors as the NiCoCr-rich c phase [20] or CoCr phase, independently reported as a tetragonal [20, 21] crystal structure. However, by TEM electron diffraction, a qualitative result in agreement just with the tetragonal phase was obtained. A Rietveld refinement method was employed to qualify this phase. It was found that these diffraction peaks corresponds to a third solid solution phase (phase C, Table 3), and its structure is close to a tetragonal r-CoCr phase according to the ICSD 102316, obtaining slight differences versus the isolated CoCr system [22]. Although the peaks group closely coincides with the CoCr phase (ICSD 102316), the solid solution phase found in this study has a high Cr, Fe and Co content, and also lower percentages of Al and Ni. According to binary alloy phase diagrams, it is known that Cr (between 54 and 66 at.%) forms a tetragonal phase with Co (σCoCr), whereas Fe in a composition between 44.5 and 50 at.%, similarly forms a tetragonal phase with Cr (σCrFe). The addition of at least 5 major elements in the studied alloys does not lead

Table 4
Structural characteristics of sintered products obtained from XRD patterns.

Alloy	Phase	Lattice parameter (nm)	Crystallite size (nm)	Lattice strain (%)
NiCoAlFeCr	BCC	0.287	78.1	0.197
	FCC	0.358	107.0	0.163
NiCoAlFeMo	BCC	0.287	40.9	0.312
	FCC	0.360	47.5	0.287
NiCoAlFeTi	BCC	0.290	35.7	0.350
	FCC	0.431	425.3	0.075

To the formation of intermetallic compounds, as might be predicted by phase diagrams; therefore the formation of solid solutions is favored.

The NiCoAlFeMo alloy is also composed by FCC and BCC (Fe-type, aFe bcc = 0.286 nm) solid solution phases (Fig. 5b). They have similar lattice parameters to those of the alloy containing Cr, 0.360 and 0.287 nm, respectively. However, the main difference is the presence of other two different solid solution phases, which were identified similar as σ-CoMo (tetragonal) and μ-CoMo (rhom-bohedral) phases, according with ICSD 102541 and 102544, respectively [23,24]. Similar solid solution phases were reported before in multi-component alloys containing Mo, after aging treatments [25,26].

The FCC solid solution phase of the NiCoAlFeTi alloy has a lattice parameter of 0.431 nm, while the BCC solid solution phase, which presents reflections corresponding to an ordered phase, shows a lattice parameter of 0.290 nm. In comparison with the alloy containing Cr, the peak positions of the BCC solid solution phase slightly shift to lower angles.

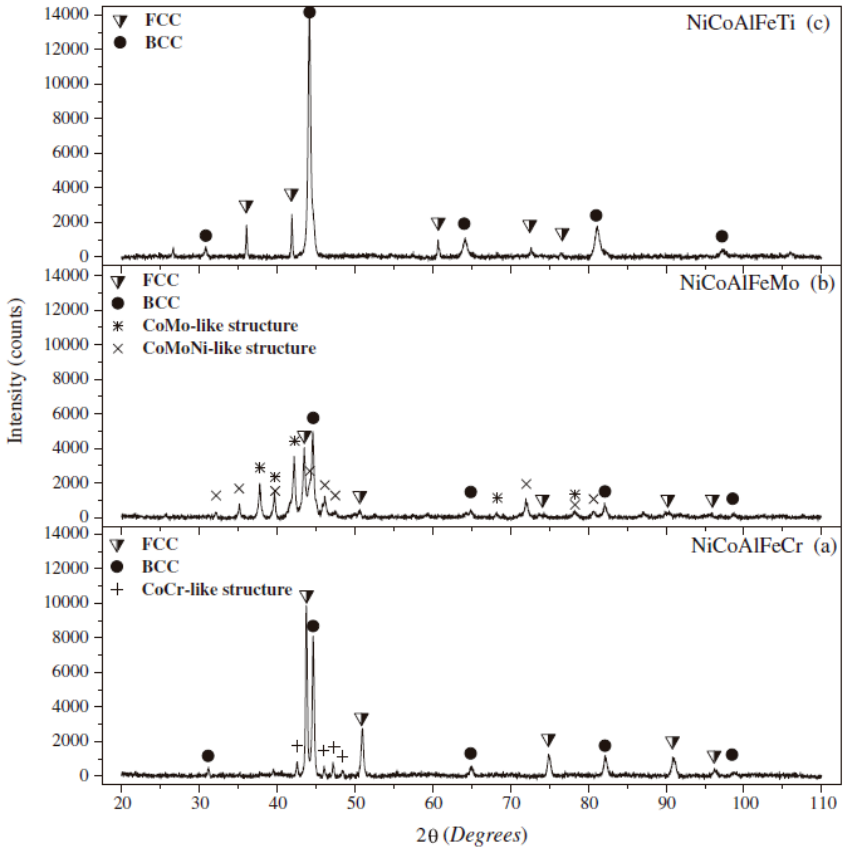

Fig. 5. XRD patterns of the sintered: (a) NiCoAlFeCr, (b) NiCoAlFeMo and (c) NiCoAlFeTi alloys.

The differences in lattice parameters must be attributed to com-position and atomic size variations.

After sintering, all the alloys undergo a significant grain growth (Table 4), nevertheless the precipitates retain a fine size and uniform distribution. On the other hand, the lattice strain values fall down because of the recovering process during the sintering stage.

Spinodal decomposition is considered as low fluctuations of the chemical composition on a large space (differs from the classical nucleation), which is characterized by large fluctuations on chemical composition in a lower space. The resulting microstructure consists of phases with similar crystal structure [27]. It was

found that there is a sideband alongside the main peaks in the X-ray diffraction pattern of the sintered specimens. This implies that the formation of phases, with minor differences in chemical composition, is due to the spinodal decomposition mechanism. The presence of spinodal decomposition has been reported in previous investigations of multi-component systems [2, 28–30].

3.4. Microhardness

The hardness test is one of the main non-destructive techniques used to determine the mechanical properties of bulk materials. The sintered specimens were examined by microhardness testing, which is one of the most simple and easiest techniques to find the tendency of mechanical properties of the studied alloys regarding to chemical composition. The obtained values of Vickers microhardness (Fig. 6) indicate that the hardest alloy is NiCoAl-FeMo (896 ± 90 HV), followed by NiCoAlFeTi (807 ± 52 HV) and NiCoAlFeCr (488 ± 82 HV).

Kao et al. [18] reported a hardness value of 484.0 ± 26 HV for a NiCoAlFeCr alloy produced by vacuum arc melting. This value is similar to that obtained in MCS with Cr additions. Shun et al.[13] investigated CoCrFeNiMox (x = 0, 0.3, 0.5, and 0.85, in molar ratio) alloys produced by arc melting and they found that the hardness increased with the Mo content, from 135 to 420 HV. On the other hand, the Co1.5CrFeNi1.5Ti0.5Mo0.1 alloy with a mean hardness of 400 HV has been reported and discussed [31, 32]. Chuang et al., investigated Al0.2Co1.5CrFeNi1.5Ti0.5 and Al0.2Co1.5CrFeNi1.5Ti alloys produced by arc melting and present hardness (HV) values of 487 ± 5 and 717 ± 13, respectively [9]. Fu et al. reported that a nanocrystalline Co0.5FeNiCrTi0.5 alloy produced by MA

and spark plasma sintering (SPS) reached a mean hardness ~860 HV [33]. This alloy is slightly harder than NiCoAlFeTi, but it is important to emphasize that it was processed by conventional sintering that is supposed to have lower mechanical performance in comparison to SPS. These values are lower than that hardness value reported for the NiCoAlFeMo. However, the processing route is different, and it is expected that nanostructures obtained by milling

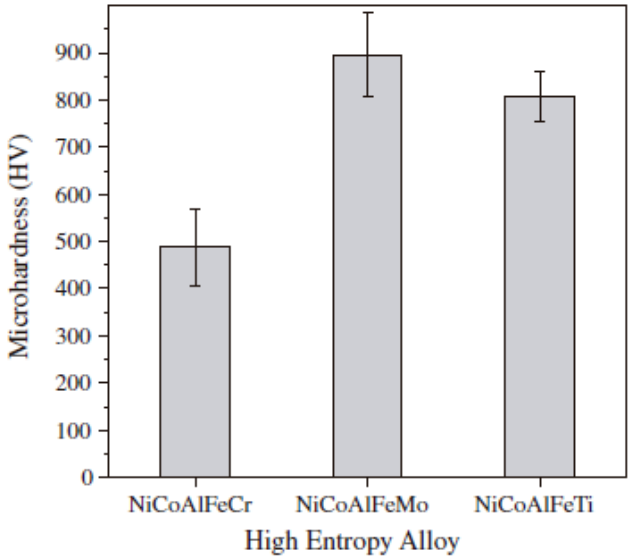

Fig. 6. Microhardness of the sintered products.

Process, which still in the order of nanometers after sintering process, have an important effect in final hardness values. The grain size in polycrystalline materials has a pronounced effect on their mechanical properties. A finer grain size material is harder and stronger due to a greater grain boundary area to impede dislocation motion. According to the results of the average grain size of sintered samples, obtained from TEM observations and X-ray line broadening, the finest grain size alloy is the one containing Mo and corresponds to the alloy with higher hardness; however this result does not correspond with MCS with Ti additions.

Even though there are different levels of solubility among the starting elements, all the phases observed in the studied alloys are composed of all those elements, the preference for the formation of solid solutions of the intermetallic compounds is evident. One of the hardening mechanism for the MCS is the solid solution hardening [34]; larger atoms such as Ti and Mo (atomic size of 0.146 y 0.139 nm, respectively) distort the lattice, acting as obstacles and improving the slipping resistance.

These variations in hardness with grain size are due to several strengthening mechanisms working in MCS at the same time, for example each alloying element has a different influence in mechanical properties. Additionally, size and distribution of second phases are factors that have an important effect in mechanical behavior.

4. Conclusion

Three multi-component systems, NiCoAlFeCr, NiCoAlFeMo and NiCoAlFeTi, produced by mechanical alloying and subsequent conventional sintering, were studied. The following conclusions were reached:

1. Microstructure and hardness of multi-component systems strongly depend on the chemical composition.

2. XRD studies showed that all as-milled powder samples present only BCC and FCC phases, while the sintered products with Cr and Mo additions present reflections corresponding to phases with structures that differ to the expected BCC or FCC structures (tetragonal, and rhombohedral structures).

3. The NiCoAlFeMo alloy reached the highest hardness, exceeded in 83% and 11% the NiCoAlFeCr and NiCoAlFeTi alloys, respectively.

4. The mechanical properties of multi-component systems are enhanced by the combination of alloying elements, the grain refinement caused by the effect of mechanical alloying, as well as the nanostructure precipitates synthesized during the sintering process.

5. Even the MCS have simple structures and are easily synthesized; several strengthening mechanisms are presented in these materials.

Acknowledgments

This research was supported by CONACYT-Red Temática de Nanociencias y Nanotecnología and Red Temática de Ciencia y Tec-nología Espaciales (0124623, 0124891, 0170224 and 0170617). The authors would like to thank the technical assistance of W. Antúnez-Flores, E. Torres-Moye, C.E. Ornelas-Gutiérrez, J.E. Ledezma-Sillas and J.M. Salinas-Gutierrez.

Reference

[1] J.W. Yeh, S.K. Chen, S.J. Lin, J.Y. Gan, T.S. Chin, T.T. Shun, C.H. Tsau, S.Y. Chang, Adv. Eng. Mater. 6 (2004) 299–303.

[2] S. Singh, N. Wanderka, B.S. Murty, U. Glatzel, J. Banhart, Acta Mater. 59 (2011) 182–190.

[3] B.S. Li, Y.P. Wang, M.X. Ren, C. Yang, H.Z. Fu, Mater. Sci. Eng. A 498 (2008) 482–486.

[4] K.B. Zhang, Z.Y. Fu, J.Y. Zhang, W.M. Wang, S.W. Lee, K. Niihara, J. Alloys Comp. 495 (2010) 33–38.

[5] K.B. Zhang, Z.Y. Fu, J.Y. Zhang, W.M. Wang, H. Wang, Y.C. Wang, Q.J. Zhang, J. Shi, Mater. Sci. Eng. A 508 (2009) 214–219.

[6] Y.J. Zhou, Y. Zhang, F.J. Wang, Y.L. Wang, G.L. Chen, J. Alloys Comp. 466 (2008) 201–204.

[7] C.-C. Tung, J.-W. Yeh, T.-T. Shun, S.-K. Chen, Y.-S. Huang, H.-C. Chen, Mater. Lett. 61 (2007) 1–5.

[8] F.J. Wang, Y. Zhang, Mater. Sci. Eng. A 496 (2008) 214–216.

[9] M.-H. Chuang, M.-H. Tsai, W.-R. Wang, S.-J. Lin, J.-W. Yeh, Acta Mater. 59 (2011) 6308–6317.

[10] Y.-S. Huang, L. Chen, H.-W. Lui, M.-H. Cai, J.-W. Yeh, Mater. Sci. Eng. A 457 (2007) 77–83.

[11] C. Suryanarayana, Prog. Mater. Sci. 46 (2001) 1–184.

[12] C.E. Lyman, Scanning Electron Microscopy, X-Ray Microanalysis, and Analytical Electron Microscopy: A Laboratory Workbook, Springer, Dordrecht, 1990.

[13] T.-T. Shun, L.-Y. Chang, M.-H. Shiu, Mater. Charact. 70 (2012) 63–67.

[14] T.B. Massalski, H. Okamoto, P.R. Subramanian, L. Kacprzak, W.W. Scott, Binary Alloy Phase Diagrams, American Society for Metals, 2001.

[15] F.J. Wang, Y. Zhang, G.L. Chen, J. Alloys Comp. 478 (2009) 321–324.

[16] R. Prescott, M.J. Graham, Oxid. Met. 38 (1992) 233–254.

[17] Y.P. Wang, B.S. Li, M.X. Ren, C. Yang, H.Z. Fu, Mater. Sci. Eng. A 491 (2008) 154–158.

[18] Y.-F. Kao, T.-J. Chen, S.-K. Chen, J.-W. Yeh, J. Alloys Comp. 488 (2009) 57–64.

[19] T.-T. Shun, Y.-C. Du, J. Alloys Comp. 479 (2009) 157–160.

[20] Y.-L. Chen, Y.-H. Hu, C.-W. Tsai, J.-W. Yeh, S.-K. Chen, S.-Y. Chang,

Mater. Chem. Phys. 118 (2009) 354–361.

[21] M.-R. Chen, S.-J. Lin, J.-W. Yeh, S.-K. Chen, Y.-S. Huang, C.-P. Tu, Mater. Trans. 47 (2006) 1395–1401.

[22] G.J. Dickins, A.M.B. Douglas, W.H. Taylor, Acta Cryst. 9 (1956) 297–303.

[23] J.B. Forsyth, L.M. d'Alte da Veiga, Acta Cryst. 16 (1963) 509–512.

[24] J.B. Forsyth, L.M. d'Alte da Veiga, Acta Cryst. 15 (1962) 543–546.

[25] T.-T. Shun, L.-Y. Chang, M.-H. Shiu, Mater. Charact. 81 (2013) 92–96.

[26] T.-T. Shun, C.-H. Hung, C.-F. Lee, J. Alloys Comp. 495 (2010) 55–58.

[27] F. Findik, Mater. Des. 42 (2012) 131–146.

[28] C.-M. Lin, H.-L. Tsai, Intermetallics 19 (2011) 288–294.

[29] S. Singh, N. Wanderka, K. Kiefer, K. Siemensmeyer, J. Banhart, Ultramicroscopy 111 (2011) 619–622.

[30] K.G. Pradeep, N. Wanderka, P. Choi, J. Banhart, B.S. Murty, D. Raabe, Acta Mater. 61 (2013) 4696–4706.

[31] Y.C. Wang, J.W. Yeh, Microstructure and Mechanical Properties of AlxCo1.5CrFeMoYNi1.5Ti0.5, in: Department of Materials Science and Engineering, National Tsing Hua University, Taiwan, 2007.

[32] Y.L. Chou, Y.C. Wang, J.W. Yeh, H.C. Shih, Corros. Sci. 52 (2010) 3481–3491.

[33] Z. Fu, W. Chen, H. Xiao, L. Zhou, D. Zhu, S. Yang, Mater. Des. 44 (2013) 535–539.

[34] Y. Zhang, Y. Zhou, X. Hui, M. Wang, G. Chen, Sci. China Ser. G: Phys.

Mech. Astron. 51 (2008) 427–437.